The July 2018 High Temperature Event in Japan Could Not Have Happened without Human-Induced Global Warming

Yukiko Imada[1], Masahiro Watanabe[2], Hiroaki Kawase[1],
Hideo Shiogama[3], and Miki Arai[2]
[1]*Meteorological Research Institute*, *Japan Meteorological Agency*, *Ibaraki*, *Japan*
[2]*Atmosphere and Ocean Research Institute*, *University of Tokyo*, *Chiba*, *Japan*
[3]*National Institute for Environmental Studies*, *Ibaraki*, *Japan*

Abstract

The high temperature event in July 2018 caused record-breaking human damage throughout Japan. Large-ensemble historical simulations with a high-resolution atmospheric general circulation model showed that the occurrence rate of this event under the condition of external forcings in July 2018 was approximately 20%. This high probability was a result of the high-pressure systems both in the upper and lower troposphere in July 2018. The event attribution approach based on the large-ensemble simulations with and without human-induced climate change indicated the following: (1) The event would never have happened without anthropogenic global warming. (2) The strength of the two-tiered high-pressure systems was also at an extreme level and at least doubled the level of event probability, which was independent of global warming. Moreover, a set of the large-ensemble dynamically downscaled outputs revealed that the mean annual occurrence of extremely hot days in Japan will be expected to increase by 1.8 times under a global warming level of 2°C above pre-industrial levels.

(**Citation**: Imada, Y., M. Watanabe, H. Kawase, H. Shiogama, and M. Arai, 2019: The July 2018 high temperature event in Japan could not have happened without human-induced global warming. *SOLA*, **15A**, 8−12, doi:10.2151/sola.15A-002.)

1. Introduction

In July 2018, Japan experienced extremely high temperature. The accumulated number of weather stations reporting extremely high daily maximum temperatures (exceeding 35°C) was more than 6000 based on the 927 stations. This heat event caused damage to human health with 1032 deaths during this period (based on the statistical summary provided by the Japanese Ministry of Health, Labor and Welfare). Human-induced global warming probably contributed to the high temperatures in Japan and other East Asian regions in recent decades (Imada et al. 2014; Imada et al. 2017). Moreover, two seasonal high-pressure systems, namely the North Pacific subtropical high (NPSH) in the lower troposphere and Tibetan high in the upper troposphere often cause warm climate in Japan (Imada et al. 2014). This two-tiered high-pressure system (double-High) was also visible in July 2018 (Figs. 1a and b). Shimpo et al. (2019) stated that the expansion of the Tibetan High to Japan was attributable to the repeated meandering of the subtropical jet stream (STJ), and expansion of the NPSH was attributable to the meridional dipole pressure pattern (the Pacific-Japan (PJ) pattern; Nitta 1987; Kosaka and Nakamura 2010) associated with enhanced convective activity around the Philippines. The meandering of the polar front jet (PFJ) also contributed to the development of the double-High in July 2018. However, experts do not have any answers on whether the double-High in 2018 was extreme compared to other such historical events. It is even more difficult to determine the extent to which human-induced global warming contributed to this event.

Attributing changes in the probability of a specific extreme event to possible causes is called event attribution (EA; Stott 2016). A set of large-ensemble model simulations under conditions with and without human-induced climate change is often utilized as an effective tool of EA. In this study, we quantitatively estimated the contribution of both human-induced global warming and the double-High toward the July 2018 high temperature event in Japan using high-resolution large-ensemble historical and non-warming simulations, the so-called d4PDF (Mizuta et al. 2017). We also estimated the occurrence of extremely hot days at each grid points in Japan owing to global warming in the near future.

2. Observational data set and large ensemble simulations

The data for tropospheric temperatures and geopotential heights was obtained from the 55-year Japanese reanalysis (JRA-55) dataset (Kobayashi et al. 2015). For the accumulated number of stations reporting extremely high temperature, we used the data source provided by JMA which is based on the automated meteorological data acquisition system (AMeDAS; approximately 927 stations at intervals of approximately 21 km) maintained by the JMA.

Our large-ensemble pairs of global and regional climate model simulations are part of the database for policy decision-making for future climate change (d4PDF) (Mizuta et al. 2017). The global climate simulations were conducted using the atmospheric general circulation model (MRI-AGCM3.2) developed by the Meteorological Research Institute, with a grid spacing of approximately 60 km (Mizuta et al. 2012). The regional climate simulations were conducted using the nonhydrostatic regional climate model (NHRCM) with a 20 km grid spacing (Sasaki et al. 2008). The regional climate simulation covered the East Asian region.

The historical simulations (HIST) were forced by the historical sea surface temperature (SST) and sea ice thickness/concentration based on COBE-SST2 (Hirahara et al. 2014) and historical anthropogenic and natural forcing agents such as greenhouse gases and solar irradiance; the RCP4.5 emission scenario was used for the period after 2006, comprising a 100-member ensemble with different initial conditions and SST perturbations from 1951 to the present. The non-warming simulations (non-W) were forced by the historical natural forcing agents and counterfactual "natural" SST and sea ice estimated by removing the warming trends observed in the 20th century. The anthropogenic forcings were fixed at a value of 1850 in the non-W (for more details, refer to Shiogama et al. 2016). In the official d4PDF, the HIST/non-W datasets of MRI-AGCM3.1 (60km resolution) cover the period from 1951 to 2010. For the regional simulations, only the HIST ensemble of NHRCM (20 km resolution) is available. Thus, we extended the calculations to July 2018 and added the downscaled calculations as a quasi-real-time product.

In this paper, the model analyses presented in Sections 3 and 4 are based on the 60 km global model. The 20 km regional climate simulations are used in Section 5 to estimate the simulated total area of locations experiencing extremely hot days.

Corresponding author: Yukiko Imada, Meteorological Research Institute, Japan Meteorological Agency, 1-1 Nagamine, Tsukuba, Ibaraki 305-0052, Japan. E-mail: yimada@mri-jma.go.jp.

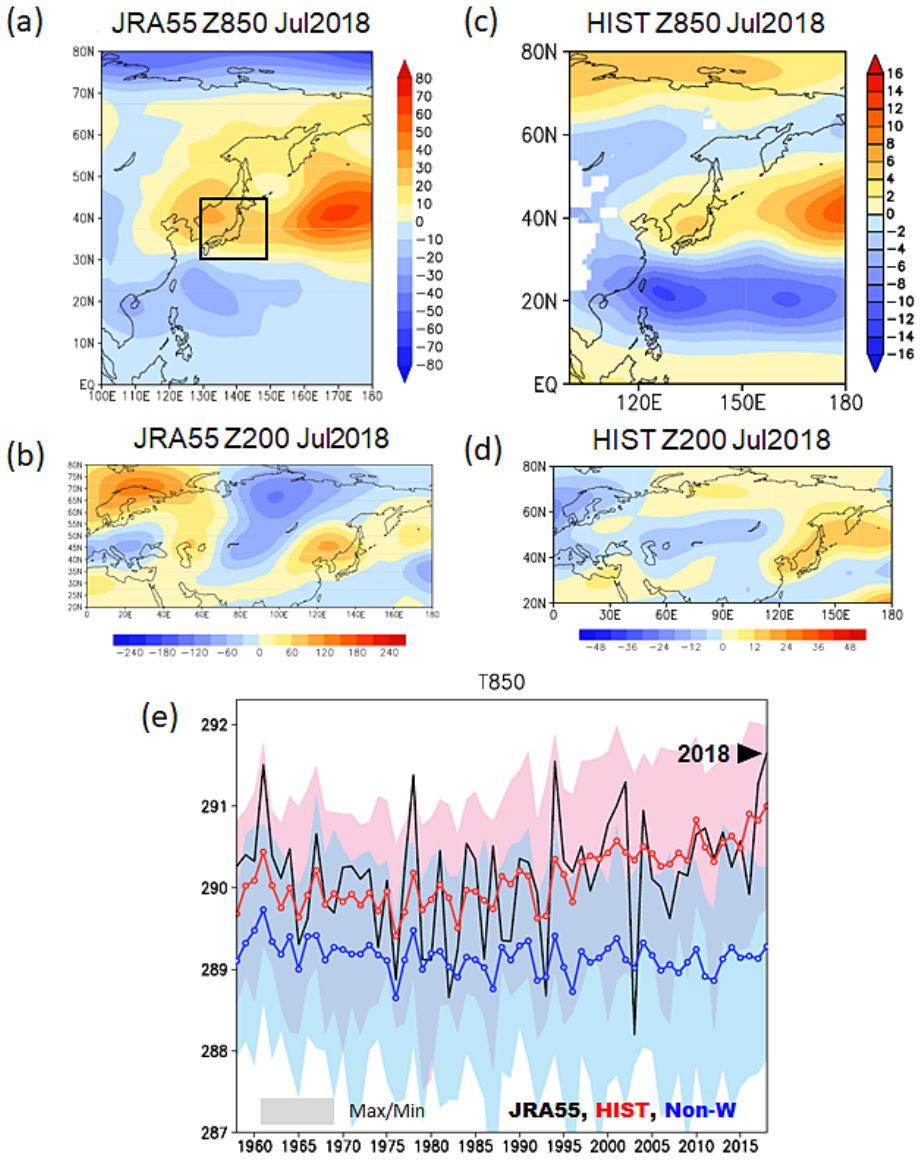

Fig. 1. Anomalies in July 2018 for (a) Z850 [m] according to JRA-55, (b) Z200 [m] according to JRA-55, (c) Z850 [m] according to HIST, and (d) Z200 [m] according to HIST. 100-member ensemble-mean anomalies are shown in (c) and (d). (e) Time series of T850 [K] averaged in 130°E−147°E and 30°N−43°N. Black: JRA-55; red: ensemble mean of HIST; blue: ensemble mean of non-W. The shadings indicate the range of all members.

3. Historical variations in temperature and the two-tiered high-pressure system

Figure 1e shows historical changes in the lower-troposphere (850 hPa) temperature (T850) in July averaged over Japan (130°E−147°E, 30°N−43°N) based on JRA-55, HIST, and non-W. Here, we used T850 to define the temperature index in place of land surface temperature because, in AGCM simulations forced by the prescribed SST, variance of surface temperature could be underestimated on small islands due to a direct impact of the surrounding SST. The JRA-55 time series shows unprecedented high temperatures in July 2018. The HIST ensemble adequately covers the historical temperature changes over Japan and the ensemble mean field reproduces record high temperatures in July 2018.

To identify the double-High events from the historical record, we performed a singular value decomposition (SVD) analysis using the upper- (200 hPa) and lower- (850 hPa) tropospheric geopotential heights (hereafter, Z200 and Z850, respectively) around Japan (See rectangles in Figs. 2b and 2d) to obtain a concurrent dominant intrinsic mode from JRA-55. Here, the area mean inside each analysis region was removed from Z200 and Z850 to obtain a relative circulation field. The first principle mode (SVD1) shows the double-High structure (Figs. 2b and 2d). The Z850 field shows the typical PJ pattern (Fig. 2b), and the Z200 field shows the Rossby wave trains along the STJ and the PFJ causing meandering of the jet streams. The patterns in Figs. 2b and 2d well represent the anomaly patterns in July 2018 (Figs. 1a and 1b), indicating that the SVD1 can capture the combined mode of the PJ pattern and the Rossby wave trains along the STJ and the PFJ. The expansion coefficient of July 2018 for Z200 (Z850) was the fourth highest (the second highest), indicating that the circulation aspect was also extreme compared to the historical record in JRA-55 (black line in Figs. 2a and 2c), although we have experienced the same level of double-High events a few times in the past. The scatter plot of the two expansion coefficients of JRA-55 (black cross marks in Fig. 2e) also confirms the extremeness of the double-High in July 2018. Hereafter, we used the two expansion coefficients as the index of the double-High. The long-term trend of the double-High index remains at the same level unlike

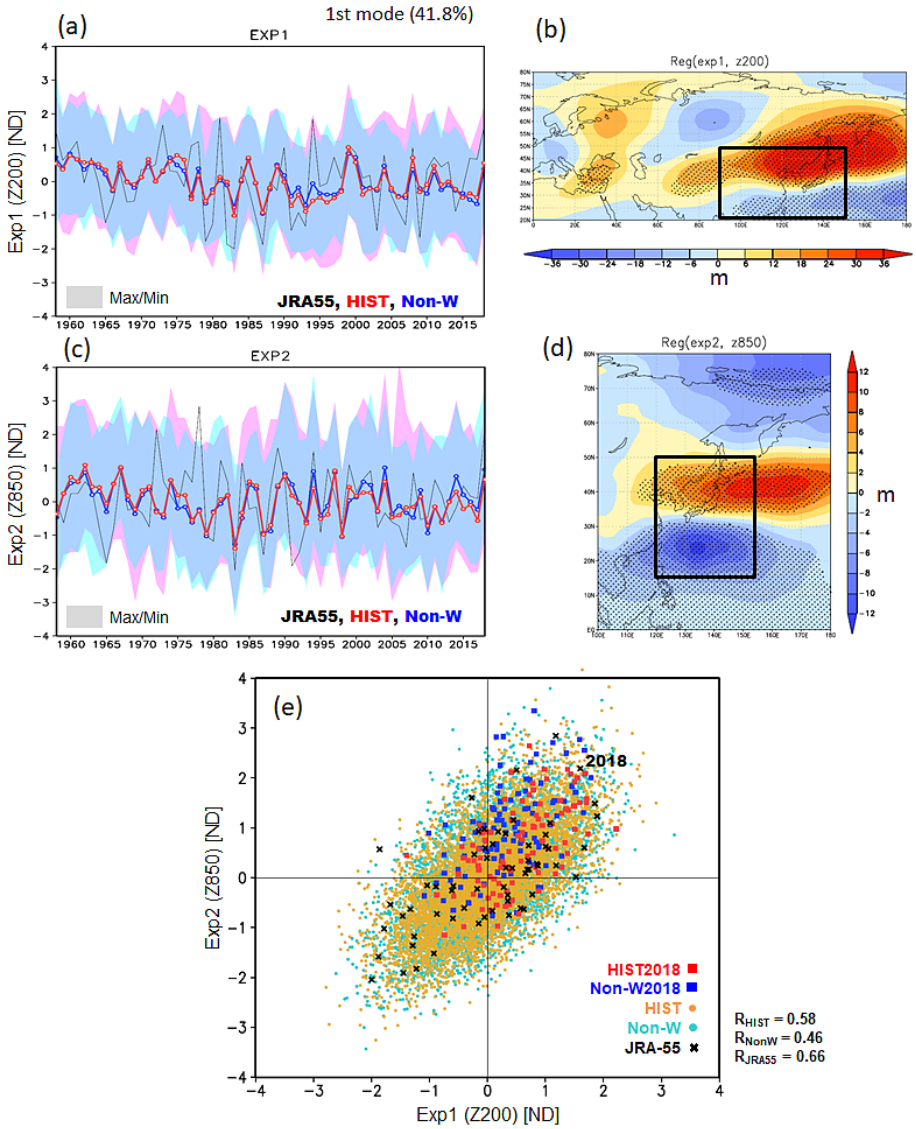

Fig. 2. SVD1 expansion coefficients normalized by each standard deviation of JRA-55 for (a) Z200 and (c) Z850 from the SVD analysis based on JRA-55 (non-dimensional). Shadings indicate the range of normalized expansion coefficients for simulations estimated by projecting each member onto each singular vector obtained from the JRA-55 records. (b) and (d) Z200 and Z850 anomaly patterns of JRA-55 regressed onto each expansion coefficient ([m], black lines of a and c), respectively. The stippling in (b) and (d) indicates the area exceeding 99% significance level by t-test. (e) Scatter plot of the SVD1 expansion coefficient for Z850 against the coefficient for Z200. The red (blue) squares denote the coefficients of HIST (non-W) in July 2018, and the dark yellow (light-blue) circles denote the coefficients of HIST (non-W) from 1958 to 2017. The black cross marks denote the coefficients of JRA-55 from 1958 to 2018 (The value of 2018 is highlighted).

the warming trend presented in Fig. 1e. Thus, the double-High condition appears to be natural variability and not affected by the human-induced climate change at this stage.

The double-High indices for the model simulations were estimated by projecting each member onto each singular vector obtained from the JRA-55 records. The obtained indices are plotted in Figs. 2a, 2c, and 2e. The ensemble means of the Z200 and Z850 indices both for HIST and non-W in July 2018 also show positive peaks (Figs. 2a and 2c). The scatter plot of the July 2018 samples (squares in Fig. 2e) also shifts to the first quadrant. These features are consistent with the fact that the ensemble-mean spatial anomaly patterns in Figs. 1c and 1d show the development of a double-High structure similar to that in the reanalysis dataset over Japan in July 2018 although the wave trains along the STJ and the PFJ are not clear in the model. Moreover, the magnitude of the ensemble-mean signals is smaller than the amplitude of anomalies in the reanalysis. This implies that the double-High pressure system in July 2018 was not purely because of the stochastic atmospheric internal variability but was partly forced by the SST, sea ice, or any other external forcing. The weak La Niña condition in July 2018 could have enhanced convection around the Philippine Sea and the development of the NPSH (Kosaka et al. 2013). The La Niña event in the preceding winter could also have a role in developing the PJ pattern in the summer through the tropical Indian Ocean warming (Xie et al. 2009; Hu et al. 2011). On the other hand, the source of the Rossby-wave propagations along the STJ and the PFJ are not easy to detect. These points will be discussed in another paper.

Again, the difference in the double-High indices between HIST and non-W is unclear (the red and blue lines in Figs. 2a and 2c), indicating that the impact of anthropogenic climate change on the double-High event is little. Note that, the results do not change when the singular vectors obtained from the SVD analysis of HIST and non-W are used to define the double-High index although the contribution rates of SVD1 based on the simulations are slightly smaller than that based on JRA-55.

4. Event Attribution study

In this section, we focus on the event probability in July 2018. Figure 3 shows the probability density functions (PDFs) of the T850 indices defined in Fig. 1. The difference in the curves for HIST (red) and non-W (blue) indicates the impact of human activity. The probability of exceeding the level of the July 2018 temperature (T850 = 18.5°C) is 19.9% (a confidence interval is 15.5−24.5% by 10th and 90th percentiles of 5000 bootstrap random sampling) for HIST, while it is 3.31×10^{-5}% (1.13×10^{-5}–5.69×10^{-5}%) for non-W. This result indicates that the warm event during July 2018 would never have happened without anthropogenic global warming. Moreover, when we considered only the subsample of HIST with a double-High system where both the expansion coefficients are positive (the first quadrant of Fig. 2e) in the SVD analysis presented in Section 3, the probability increased to 24.6% (20.0−29.4%) as shown in Fig. 3 with the magenta-dashed curve). On the other hand, when we considered only the subsample without a double-High system where both or one of the expansion coefficients are negative (the second, third, and forth quadrant of Fig. 2e), the probability reduced to 12.2% (7.62−17.1%) as shown with the orange-dashed curve in Fig. 3. Note that, a case "with" a double-High defined here does not necessarily correspond to a case as strong as the double-High in July 2018 but includes weaker double-High systems. Therefore, the double-High structure also had an important role in at least doubling the risk of the 2018 high temperature event, which is independent of anthropogenic impacts.

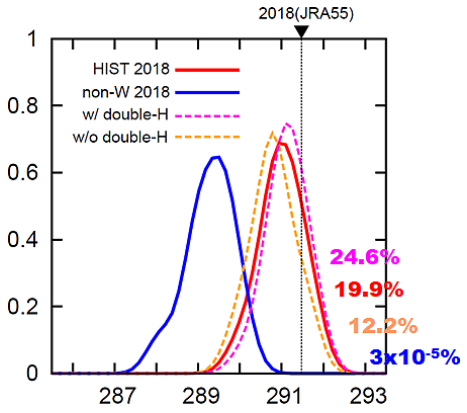

Fig. 3. PDFs for T850 [K] over Japan. The red- (blue-) solid line is the result of the July 2018 ensemble simulations of HIST (non-W). The magenta-dashed and orange-dashed line was estimated from the members with and without the double-High system in the HIST run, respectively.

5. Occurrence of extremely hot days at each grid points in Japan

Using large-ensemble high-resolution (20 km mesh) regional products, we can estimate the impact of human-induced global warming to regional-scale extreme events. As an example, Fig. 4a presents the difference in the number of extremely hot days in July 2018 between HIST and non-W at each grid point of the regional model. Here, the JMA defined the threshold for extremely high temperatures as 35.0°C, which is approximately the 99-percentile value of the total daily maximum temperature observations during 2010−2017. For the model simulations, we used the 99-percentile value of HIST in the same period (32.9°C) as the threshold because the simulated grid-mean temperature underestimated the temperature observed at the sites. Figure 4a shows a pronounced increase in the extremely hot days in the populated areas of Japan during July 2018 due to the anthropogenic climate change. Further details of the regional aspects of the July 2018 warm event will be presented in another paper.

The large-ensemble regional products are also available to project near-future changes in regional extremes. We presented the density of the scatter plot of the mean annual occurrence of extremely high temperatures (vertical axis) relative to the global annual-mean surface air temperature (horizontal axis) using the HIST and non-W simulations (Fig. 4b). The mean annual occurrence (unit: days/year/grid) was estimated as accumulated fraction of grid points experiencing an extremely high daily maximum temperature within each year among all the grid points in Japan (1350 grid points) throughout each year. For reference, mean annual occurrence estimated from the AMeDAS sites (total 927 sites) and global-mean surface temperature provided by the JMA were also plotted for the period after 2010. The white curve indicates the cumulative distribution function (CDF) of the daily maximum temperatures in Japan for all the grid points and days of non-W from 1951 to 2017 in assuming that the PDF of daily max-

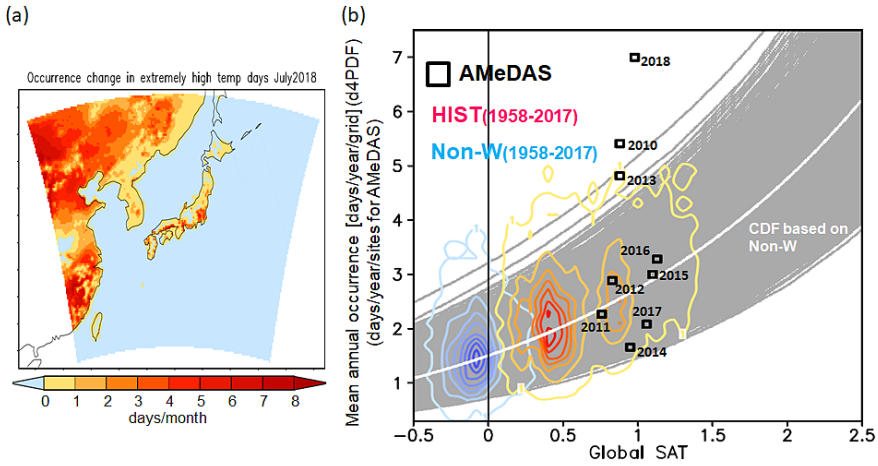

Fig. 4. (a) Difference in the number of extremely hot days in July 2018 between HIST and non-W at each grid point of the regional model [days/month]. Ensemble-mean values are plotted. (b) Density of the scatter plot [counts/bin] of the mean annual occurrence [days per year] of extremely high daily maximum temperature per the total number of grid points of Japan against the global annual-mean surface air temperature [K]. We divided the plot area into 1750 bins; each bin is defined as a space with 0.06 K (horizontal) and 0.2 days/year/grid (vertical). Warm-color (cold-color) contours are results from all members and years (1958−2017; the results of 2018 are not plotted because the simulations ended at July 2018) from the HIST (non-W) run with an interval of 20 (40) counts per bin starting at 1. For reference, the mean annual occurrence estimated from the AMeDAS sites after 2010 are also plotted, indicated by open-black squares. The white curve indicates the CDF estimated from surface temperatures in Japan for all grid points and days of the non-W run from 1951 to 2017, and the gray curves indicate 5000 CDFs generated by the bootstrap resampling.

imum temperature for all grid points of Japan shifts in a positive direction in proportion to the global-mean surface temperature with a fixed shape. The CDF curve well represents the combined plots for HIST and non-W, indicating an average level of the mean annual occurrence of extremely high temperatures per year at each warming stage. Since the last decade, the warming level across the world has been at approximately 1°C. Thus, in recent years, it is not surprising that the mean annual occurrence of high temperatures is equal to almost 2.7 days per year per grid. Again, the extremely high temperature event in 2018 was an extraordinary situation in which extreme temperatures were experienced almost seven days per year per sites of AMeDAS on average.

Using the CDF curve shown in Fig. 4b, we could project near-future trends regarding the mean annual occurrence of high temperatures. Under a global warming level of 1.5°C (2°C), the average days that could experience high temperatures is estimated to be approximately 3.6 (4.8) days/year/grid; such a fraction was observed only a few times in the past.

6. Discussion and conclusion

This paper presented a quantitative estimate of the contribution of human-induced climate change to the extremely high temperature experienced in Japan in July 2018 using a large-ensemble database, the so-called d4PDF. By comparing the event probabilities between the historical (realistic) and non-warming (without human impact) ensemble sets, we concluded that the warm event in July 2018 would never have happened without human-induced climate change.

Furthermore, this is an initial attempt to quantify not only the human-induced effect but also the contribution of specific natural variabilities. In the July 2018 case, the double-High system was the main natural variability, which is independent of anthropogenic effects. We separated the 2018 simulations into members with and without double-High development and found that the probability of extremely high temperatures at least doubled owing to the existence of the double-High pressure system in July 2018.

The July 2018 high temperature event caused serious damage to human lives in Japan. We have the responsibility of reporting to what extent this disastrous event was attributable to human activity to provide concrete results and alert people to take all possible steps to minimize future damage associated with anthropogenic global warming. To emphasize this fact, we also projected near-future trends of the mean annual occurrence of extremely hot days in Japan. Our results suggested that the extremely high temperatures experienced only a few times in the past could become a usual situation with warming levels of 1.5 or 2°C in the next few decades.

Note that, model dependency and uncertainty in the boundary conditions of non-W are big issues in an EA research. There is an international multi-model intercomparison project for EA to address these issues (Stone 2013). Although the EA simulations of d4PDF has a higher resolution and a longer-term coverage of periods than the other state-of-the-art EA databases in the world, the weak point is in consideration of the uncertainties. Huge computational costs limit the goal. The results in this paper appears to be the best estimates within our current capabilities. The remaining issues will be explored in the future.

This is a prompt report, and we skipped the discussion regarding how the development of the double-High system (that is, the PJ pattern and the Rossby wave-like patterns) in July 2018 was forced by large-scale factors. The specific SST in 2018 possibly had a role in forming the double-High system. Further discussions regarding this issue will be reported in future papers.

Acknowledgements

We are grateful to M. Mori, and C. Takahashi for their cooperation. This work was supported by the TOUGOU program of the Japanese Ministry of Education, Culture, Sports, Science and Technology (MEXT). This study utilized the d4PDF, which was produced using the Earth Simulator as "Strategic Project with Special Support" of JAMSTEC under corporations among the programs of SOUSEI, TOUGOU, and SI-CAT, which all were sponsored by the MEXT, Japan. This study was partly supported by Japan Science and Technology Agency (JST) and Japan Society for the Promotion of Science (JSPS) Grants-in-Aid for Scientific Research (KAKENHI) Grant Numbers 18K19951 and 18K03749.

Edited by: Y. Kosaka

References

Hirahara, S., M. Ishii, and Y. Fukuda, 2014: Centennial-scale sea surface temperature analysis and its uncertainty. *J. Climate*, **27**, 57−75.

Hu, K., G. Huang, and R. Huang, 2011: The Impact of tropical Indian Ocean variability on summer surface air temperature in China. *J. Climate*, **24**, 5365−5377.

Imada, Y., and co-authors, 2014: The contribution of anthropogenic forcing to the Japanese heat waves of 2013. *Bull. Amer. Meteor. Soc.*, **95**, S52−S54.

Imada, Y., and co-authors, 2017: Climate change increased the likelihood of the 2016 heat extremes in Asia. *Bull. Amer. Meteor. Soc.*, **97**, S97−S101.

Kobayashi, S., and co-authors, 2015: The JRA-55 Reanalysis: General specifications and basic characteristics. *J. Meteor. Soc. Japan*, **93**, 5−48.

Kosaka, Y., and H. Nakamura, 2010: Mechanisms of meridional teleconnection observed between a summer monsoon system and a subtropical anticyclone. Part I: The Pacific-Japan pattern. *J. Climate*, **23**, 5085−5108.

Kosaka, Y., S.-P. Xie, N.-C. Lau, and G. A. Vecchi, 2013: Origin of seasonal predictability for summer climate over the Northwestern Pacific. *PNAS*, **110**, 7574−7579.

Mizuta, R., H. Yoshimura, H. Murakami, M. Matsueda, H. Endo, T. Ose, and A. Kitoh, 2012: Climate simulations using MRI-AGCM3.2 with 20-km grid. *J. Meteor. Soc. Japan*, **90A**, 233−258.

Mizuta, R., and co-authors, 2017: Over 5000 years of ensemble future climate simulations by 60 km global and 20 km regional atmospheric models. *Bull. Amer. Meteor. Soc.*, **98**, 1383−1398.

Nitta, T., 1987: Convective activities in the tropical western Pacific and their impact on the Northern Hemisphere summer circulation. *J. Meteor. Soc. Japan*, **65**, 373−390.

Sasaki, H., K. Kurihara, I. Takayabu, and T. Uchiyama, 2008: Preliminary experiments of reproducing the present climate using the non-hydrostatic regional climate model. *SOLA*, **4**, 25−28.

Shimpo, A., K. Takemura, S. Wakamatsu, H. Togawa, Y. Mochizuki, M. Takekawa, S. Tanaka, K. Yamashita, S. Maeda, R. Kurora, H. Murai, N. Kitabatake, H. Tsuguti, H. Mukougawa, T. Iwasaki, R. Kawamura, M. Kimoto, I. Takayabu, Y. Takayabu, Y. Tanimoto, T. Hirooka, Y. Masumoto, M. Watanabe, K. Tsuboki, and H. Nakamura, 2019: Primary factors behind the Heavy Rain Event of July 2018 and the subsequent heat wave in Japan. *SOLA*, **15A**, in press, doi:10.2151/sola.15A-003.

Shiogama, H., and co-authors, 2016: Attributing historical changes in probabilities of record-breaking daily temperature and precipitation extreme events. *SOLA*, **12**, 225−231.

Stone, D. A., 2013: Boundary conditions for the C20C Detection and Attribution project: The ALL-Hist/est1 and NAT-Hist/CMIP5-est1 scenarios. International CLIVAR C20C+ Detection and Attribution Project, 18pp. (Available online at https://portal.nersc.gov/c20c/input_data/C20C-DandA_dSSTs_All-Hist-est1_Nat-Hist-CMIP5-est1.pdf)

Stott, P. A., 2016: Attribution of extreme weather and climate-related events. Wiley Interdisciplinary Reviews: Climate Change, **7**, 23−41.

Xie, S. P., K. M. Hu, J. Hafner, H. Tokinaga, Y. Du, G. Huang, and T. Sampe, 2009: Indian Ocean capacitor effect on Indo-western Pacific climate during the summer following El Niño. *J. Climate*, **22**, 730−747.

Manuscript received 22 February 2019, accepted 23 April 2019
SOLA: https://www.jstage.jst.go.jp/browse/sola/